A Polymer Membrane Containing Fe^0 as a Contaminant Barrier

Tsutomu Shimotori,[†] Eric E. Nuxoll,[‡] Edward L. Cussler,[‡] and William A. Arnold[†]*

[†]Department of Civil Engineering, University of Minnesota, 500 Pillsbury Dr. SE, Minneapolis, MN 55455

[‡]Department of Chemical Engineering and Materials Science, University of Minnesota, 421 Washington Ave. SE, Minneapolis, MN 55455

*Author to whom correspondence should be addressed

Email: arnol032@tc.umn.edu
Phone: 1-612-625-8582
Fax: 1-612-626-7750

Revised manuscript submitted to *Environmental Science & Technology*

November 3, 2003

Abstract

A polyvinyl alcohol (PVA) membrane containing iron (Fe^0) particles was developed and tested as a model barrier for contaminant containment. Carbon tetrachloride, copper (Cu^{2+}), nitrobenzene, 4-nitroacetophenone, and chromate (CrO_4^{2-}) were selected as model contaminants. Compared with a pure PVA membrane, the Fe^0/PVA membrane can increase the breakthrough lag time for Cu^{2+} and carbon tetrachloride by more than 100 fold. The increase in the lag time was smaller for nitrobenzene and 4-nitroacetophenone which stoichiometrically require more iron and for which the PVA membrane has a higher permeability. The effect of Fe^0 was even smaller for CrO_4^{2-} because of its slow reaction. Forty-five percent of the iron, based on the content in the dry membrane prior to hydration, was consumed by reaction with Cu^{2+} and 19 % by reaction with carbon tetrachloride. Similarly, 25 %, 17 %, and 6 % of the iron was consumed by nitrobenzene, 4-nitroacetophenone, and CrO_4^{2-}, respectively. These percentages approximately double when the loss of iron during membrane hydration is considered. The permeability of the Fe^0/PVA membrane after breakthrough was within a factor of three for that of pure PVA, consistent with theory. These results suggest that polymer membranes with embedded Fe^0 have potential as practical contaminant barriers.

Introduction

Membranes composed of high-density polyethylene (HDPE) or polyvinyl chloride (PVC) are often used as barriers in landfills and in contaminated subsurface environments (1, 2). Containment or stabilization of contamination is the goal at these sites. Leakage of contaminants through the polymer barrier, however, occurs frequently, and such leakage

is a common sediment and groundwater contamination source (3, 4). For example, contamination associated with landfills accounts for 15 % of the current National Priority List (NPL) sites (5). The leakage may be caused by physical failure of the barrier or diffusion of contaminants through the barrier material (6-8). Although polymer geomembranes are relatively impermeable, organic solvents can diffuse through them much faster than inorganic chemicals (1). For example, Rowe et al. (9, 10) measured the diffusion of methylene chloride into an HDPE membrane and estimated its diffusion coefficient in the HDPE matrix (2×10^{-12} m^2/s) to be about 300 times larger than the value for chloride (6×10^{-15} m^2/s).

One possible remedy for contaminant diffusion through membrane barriers is to incorporate reactive materials into the polymer so that the contaminants are degraded or immobilized within the membrane. These processes dramatically increase the lag time for contaminant breakthrough and extend barrier lifetimes (11). In this research, polyvinyl alcohol (PVA) membranes containing iron (Fe^0) particles were developed and tested as model barriers for a variety of environmental contaminants. PVA was selected as a model because it is easy to synthesize and has a high permeability which allows quick measurements of lag time; PVA is not realistic in practical containment applications. Iron was selected as the immobilized reactant because it reduces oxidized contaminants such as chlorinated solvents (*e.g.,* 12-19), nitroaromatic compounds (20, 21), and heavy metal ions (*e.g.,* 22-28). Carbon tetrachloride, copper (Cu^{2+}), nitrobenzene, 4-nitroacetophenone, and chromate (CrO_4^{2-}) were selected as model contaminants.

Theory

The expected increases in breakthrough or lag time for Fe^0-containing membranes are based on equations developed previously and are briefly reviewed here. The theory for diffusion through a membrane without reaction predicts that the downstream concentration changes as (11, 29):

$$\frac{C_{down}}{C_{up}} = \frac{PA}{LV_{down}}\left(t - t_{lag}\right) \tag{1}$$

$$\text{where } t_{lag} = \frac{L^2}{6D} \tag{2}$$

and where C_{down} and C_{up} are the contaminant concentrations downstream and upstream of the membrane, respectively; D is the diffusion coefficient for the selected contaminant in the membrane; P is permeability of the membrane to the contaminant, equal to HD; H is the membrane-water partition coefficient for the contaminant into the membrane; L is the membrane thickness; V_{down} is the volume of the downstream compartment; A is the cross-sectional area of the membrane available for diffusion; and t and t_{lag} are time and breakthrough lag time, respectively. Equations 1 and 2 are derived assuming that C_{up} is constant and that the volume of the upstream compartment is very large. Similar equations for other assumptions are easily derived.

For a membrane containing a reactive material that consumes contaminants irreversibly, the corresponding equation again has the form of eq 1 but with a different expression for the lag time (11):

$$t_{lag} = \frac{L^2 C_0}{2\nu P C_{up}} \tag{3}$$

where C_0 is the initial concentration of the reactive material, and ν is the stoichiometric coefficient of the reaction. For this work, ν is assumed to be 1 for Cu^{2+} (24) and carbon tetrachloride (13), 3 for nitrobenzene (20) and 4-nitroacetophenone (21), and 1.5 for CrO_4^{2-} (26). Equation 3 assumes an instantaneous reaction, i.e. the reaction is much faster than diffusion through the membrane. Yang et al. (11) demonstrated that the breakthrough lag time for various acids through membranes containing ZnO obeyed eq 3.

Ideal breakthrough curves for membranes with and without a reactive material are illustrated in Figure 1. In general, equations 1-3 are approximations, valid at small times before much contaminant penetration has occurred. These small times are important from an environmental viewpoint, as they allow predictions of initial contaminant fluxes through the barrier material. At longer times, the downstream concentration does not follow these relations, but becomes non-linear, as shown in Figure 1. Equations 1-3 form the basis for analyzing our experiments as described below.

Experimental

The following chemicals were used without further purification: ferric chloride ($FeCl_3 \cdot 6H_2O$, 99.67 %, Fisher); sodium borohydride ($NaBH_4$, 98 %, Aldrich); PVA (Elvanol 71-30, Dupont); methanol (99.95 %, Pharmco); carbon tetrachloride (99.97 %, Sigma); chloroform (99.9 %, Sigma); methylene chloride (99.9 %, Fisher); C_1-C_6 paraffin gas standard (1000 ppm each in N_2, Matheson Tri-Gas); pentane (98 %, Fisher); cupric chloride ($CuCl_2 \cdot 2H_2O$, 99 %, Fisher); nitrobenzene (99 %, Aldrich); 4-nitroacetophenone (98 %, Aldrich); perchloric acid (70 %, Alfa Aesar); potassium dihydrogen phosphate (100 %, Fisher); potassium hydrogen phosphate (100 %, Mallinckrodt); sodium chromate (Na_2CrO_4,100 %, Fisher); bathocuproinedisulfonic acid disodium salt hydrate (Aldrich);

hydrochloric acid (37.4 %, Mallinckrodt); citric acid monohydrate (100 %, Mallinckrodt); sodium hydroxide (50-52 % solution, Titristar); hydroxyl amine hydrochloride (99 %, Aldrich); FerroZine (97 %, Aldrich); acetic acid (100 %, Mallinckrodt), ammonium hydroxide (29.7 % solution, Mallinckrodt); Tris[hydroxymethyl]aminomethane hydrochloride (Tris, 99 %, Sigma-Aldrich); sodium chloride (100 %, Mallinckrodt); phosphoric acid (85 %, EM Science); and diphenylcarbazide (0.5 % in acetone, LabChem Inc.). All aqueous solutions were prepared with deoxygenated Milli-Q (Millipore) water.

The membranes were prepared in an anaerobic chamber (7 % H_2/93 % N_2, Coy Laboratory Products) to prevent unwanted oxidation of Fe^0. Nanoparticles of Fe^0 were synthesized by mixing 0.1 M aqueous solutions of $FeCl_3 \cdot 6H_2O$ and $NaBH_4$ as described previously (17). Minute, black particles were produced. A study has shown that nanoparticles of Fe^0 synthesized in a similar manner contained approximately 4 % boron by mass (30), but we simply refer to the nanoparticles synthesized here as nanoparticles of Fe^0. After the reaction was complete, the particles were rinsed with deoxygenated water to remove any residual BH_4^- and BO_3^{3-} that could disrupt cross-linking of the PVA. Scanning electron micrographs (SEM, JEOL 6500) revealed that the particles were largely spherical with diameters between 100 and 200 nm (Supporting Information).

A PVA solution was prepared by adding 2.5 g of PVA to 30 mL of water. The mixture was heated to near boiling while stirring until a completely transparent solution was obtained. After the solution was cooled and degassed under vacuum, nanoparticles of Fe^0 were mixed into the solution using an ultrasonic homogenizer (Cole-Parmer). The mixture was cast on a smooth Teflon block, leveled with a doctor blade (Mitutoyo), and

allowed to dry. After drying, the membrane was heated at 150 °C in an oven flushed with N_2 gas for 1 hour to lightly crosslink the polymer. The pure PVA membranes were synthesized in a similar manner but without the addition of Fe^0. Iron content in each synthesized Fe^0/PVA membrane was determined by the FerroZine method (31-33) after dissolving the iron particles from the membrane with Aqua Regia (34). The surfaces of Fe^0/PVA membranes observed by SEM (Figure 2) show clusters of Fe^0 evenly scattered in the membrane. The clusters are 1-2 μm in diameter, and each cluster consists of smaller Fe^0 particles (100-200 nm in diameter).

The membrane thickness was measured after overnight hydration using a micrometer (Mitutoyo). Local variation of the membrane thickness was typically ±10 %, and the average value of five measurements per membrane sample is reported. The thicknesses used ranged from 25 to 379 μm. These small thicknesses allow quick testing of the membranes. These membranes are much thinner than typical landfill liners, which are more than 1.5 mm thick (35).

Solute breakthrough across each membrane was tested with a diaphragm-cell diffusion apparatus. When the pure PVA membranes were tested, the apparatus had two closed-ended Pyrex cells (each cell volume = 11-16 mL), placed as shown in Figure 3(a). The membrane mounted between the two cells had an area for diffusion 2.54 cm in diameter. Each cell was stirred with a Teflon-coated stir bar and a magnetic stirplate. For carbon tetrachloride, a methanol spike solution containing 406 mM carbon tetrachloride was injected into the upstream cell to initiate the experiment. For the other test compounds, an aqueous solution containing the target contaminant was poured into the

upstream cell to begin. The downstream concentration was monitored by collection of aqueous samples (usually 10 μL each).

When Fe^0/PVA membranes were tested, the apparatus shown in Figure 3(b) was used. A fresh solution of each contaminant was continuously fed to the upstream cell by a peristaltic pump (MasterFlex, Cole-Parmer) to maintain a constant upstream concentration. For carbon tetrachloride, this feed solution was maintained near its saturated concentration (≈ 4500 μM) by keeping the solution in contact with liquid-phase carbon tetrachloride. For the other test compounds, the concentration of the feed solution ranged from 1000-5000 μM. Aqueous samples were taken from the two cells at appropriate intervals to monitor the contaminant concentration. For the measurement of dissolved iron concentration, 200 μL samples were taken from each of the two cells and the effluent beaker. All solutions were buffered at pH 7.2 with Tris.

Analytical methods depended on the particular solute. Carbon tetrachloride was analyzed via gas chromatography (Trace GC, ThermoQuest) with electron capture detection (ECD) and a DB-1 column (30 m × 0.32 mm ID × 5 μm film thickness, J&W Scientific) after extraction using pentane. The degradation products in selected samples were quantified with a flame ionization detector (FID) and a GS-GasPro column (30 m × 0.32 mm ID, J&W Scientific). Concentrations of Cu^{2+} and CrO_4^{2-} were determined by the bathocuproine method (36) and the diphenylcarbazide method (36), respectively, using a UV-visible spectrophotometer (UV-1601PC, Shimadzu). Nitrobenzene and 4-nitroacetophenone were measured via HPLC (LC Module 1 plus, Waters) with a Discovery® RP Amide C16 column (15 cm × 4.6 mm ID × 5 μm film thickness, Supelco). The solvent mixture was 60 % methanol and 40 % pH 7 potassium phosphate

buffer and was operated in an isocratic mode (1 mL/min). A detector wavelength of 260 nm was used. Dissolved iron was quantified using the FerroZine method (31-33).

Results

Pure PVA membranes

We first present diffusion of a solute through pure PVA membranes. Carbon tetrachloride, selected as a model contaminant, shows typical breakthrough curves for two membranes of different thickness in Figure 4. These curves are characterized by a slope and an intercept. The slopes equal $\frac{PA}{LV_{down}}$, which is a measure of the steady-state flux of carbon tetrachloride. If these slopes are normalized by A and V_{down}, the permeance, $\frac{P}{L}$, is calculated. The results in Figure 5 show that this permeance is roughly proportional to the reciprocal of the membrane thickness, supporting the analysis in eq 1. Possible reasons for the scatter of the data are stretching of the membrane, local variation of membrane thickness, and undetected pinholes.

The x-intercepts in Figure 4 are the lag times, expected from eq 1 to be proportional to the square of the membrane thickness. Although the lag times show a systematic increase with increasing membrane thickness, they are too small (< 2 min) to be precisely determined for most non-reactive membranes used in this study.

Fe^0/PVA membranes

Data for the experiments using Fe^0/PVA membranes are again presented as breakthrough curves, as shown in Figure 6 and summarized in Table 1. The data in Figures 6a-e for the pure PVA membranes, shown as solid points, have been adjusted with respect to L and C_{up} so that the two curves can be directly compared (Supporting

Information). The data given in Table 1 for the pure PVA membranes are the uncorrected values. As before, each curve is characterized by its slope and intercept. The slope of the dashed lines, obtained by regression of data near the beginning of the breakthrough, should be equal to $\frac{C_{up}PA}{LV_{down}}$ if the membrane is no longer reactive at this point.

Clear increases in the lag time are shown for carbon tetrachloride and Cu^{2+} in Figures 6a-b. The lag times shown for Fe^0/PVA membranes against carbon tetrachloride and Cu^{2+} are 352 min and 374 min, respectively, while the corresponding lag times for pure PVA membranes are respectively 1.4 min and 1.0 min (after adjustments for L and C_{up}). The breakthrough for nitrobenzene shows a smaller increase caused by the iron incorporation. The breakthrough lag time for the Fe^0/PVA membrane against nitrobenzene is 53 min, while it is 0.45 min for the pure PVA membrane (again after adjustments). There are two obvious reasons for the smaller effect. First, nitrobenzene requires more Fe^0 for reduction ($\nu = 3$) compared with carbon tetrachloride and Cu^{2+} ($\nu = 1$). Second, the permeability of the membrane to nitrobenzene is higher than for the other two compounds, which also decreases the lag time (see eq 3).

The lag times in reactive membranes are predicted to be independent of reaction kinetics (37). To test this prediction 4-nitroacetophenone was selected as a model contaminant. 4-Nitroacetophenone reacts faster with Fe^0 than nitrobenzene does (21). As shown in Figure 6(d), the breakthrough lag time for 4-nitroacetophenone diffusing across the Fe^0/PVA membrane is 46 min, close to that for nitrobenzene through a similar Fe^0/PVA membrane and thus consistent with the prediction. The lag for 4-nitroacetophenone is 0.65 min for the pure PVA membrane (after adjustments).

The breakthrough for CrO_4^{2-} is affected less by the iron incorporation. The breakthrough lag time for the pure PVA membrane is 7 min (after adjustments), while it is 87 min for the Fe^0/PVA membrane. Batch experiments show that CrO_4^{2-} reacts very slowly when its concentration is high (*e.g.,* > 1000 μM), probably because of deposition of Cr_2O_3 on the iron surface (26, 38). The large lag time for the pure PVA membrane, which is reproducible, may reflect reaction of CrO_4^{2-} with the PVA itself to form an ester (39, 40).

To investigate possible deposition of the heavy metals, we measured the chemical composition on the Fe^0/PVA membrane surface after exposure to the copper and chromate solutions. The spectra showed the presence of Cu and Cr on the membranes after reaction with Cu^{2+} and CrO_4^{2-}, respectively (Supporting Information).

The permeability of the Fe^0/PVA membranes to the selected contaminants ranged from 0.5 to 3 times that of the pure PVA. In general, the measured permeability of the reactive membranes was higher than that of the unmodified ones (Table 1). Ideally, the permeability of the membrane should not be affected by the incorporation of Fe^0 (11). Possible reasons for the observed deviation are discussed below.

To assess the significance of the reaction between Fe^0 and water as a competing reaction during the contaminant breakthrough experiments, dissolved iron concentrations were measured in two diaphragm-cell experiments, one with carbon tetrachloride and the other without carbon tetrachloride. To complete an iron mass balance, the dissolution of iron during the hydration process prior to the experiments was also measured. The duration of hydration was 23-27 hours and the diaphragm-cell experiments were 9.75 hours. The iron mass balance is based on the exposed area in the diffusion experiment.

The results showed that 40-47 % of the iron (based on the iron content in the dry membrane prior to hydration) dissolved during the hydration process, while the dissolution of the iron during the diffusion experiment was much smaller (only 5 % relative to the hydration-related loss). No difference in iron dissolution was observed between the two diaphragm cell experiments (with and without carbon tetrachloride).

Discussion

The results above show that the breakthrough lag time of polymer membranes used as contaminant barriers can potentially be dramatically increased by incorporation of reactive groups or materials within the polymer material. Although the choice of Fe^0/PVA system was designed to permit experiments to be conducted over short time scales, we expect that improvements in the barrier properties of PVA can be easily secured for other polymers such as polyethylene. This expectation has considerable experimental support from this work, and many other reagent choices are possible.

The results with the Fe^0/PVA membranes show substantial increases in the lag time before there is significant permeation through the barriers. For copper, the lag is increased 100 to 1000 fold; for carbon tetrachloride, it rises over 150 fold; for the nitroaromatics, 20 to 100 fold. The lag time increased only 13 fold for chromate, a solute for which little reaction is expected. Once the membrane is broached, the leak rate is regulated by a permeability which typically changes by less than a factor of two, but up to a factor of three (based on the slope of the breakthrough curve) from a non-reactive membrane.

The observed changes in permeability merit further discussion, as the permeability influences further analysis of the lag time data. When hydrated, PVA is 50%

water (pore space), leading to its high permeability. For a membrane containing 1.25 M iron, calculations reveal that the void volume would increase approximately 1% upon complete dissolution of the iron nanoparticles. Thus, changes in permeability of the membrane due to Fe^0 dissolution should be minimal. The larger changes in permeability observed suggest that other changes in the membrane chemistry and geometry are occurring. The dissolution of the iron could lead to a shunt forming through the membrane by connecting pores that already exist in the PVA matrix. As shown in Figure 2, the iron is not completely dispersed in the membrane and forms 1-2 μm clusters of smaller nanoparticles. Their dissolution can be envisioned to provide a shortcut across a 100-200 μm barrier, which leads to the higher permeability. Such pore connectivity is much less likely in polymers (i.e. HDPE or PVC) used for practical barriers. When developing these practical membranes, however, observed changes in permeability for the reactive membranes will be an important piece of information in determining optimum Fe^0 loadings to prevent shunt formation, and thus averting poor membrane performance after contaminant breakthrough.

Because permeability provides a reference value for lag time calculations (eq 3), subsequent analyses assume that the appropriate values of *P* to use in the interpretation of the lag time results are those measured for the pure PVA membranes. For each compound, multiple experiments with pure PVA films were run. The selected *P* for each contaminant is the lowest, reproducible value measured for the PVA membranes, which we deem to be from membranes with the fewest possible number of defects. These values are those reported in Table 1.

Despite the variations in permeability, our results demonstrate that the performance (i.e. lag time) of a contaminant barrier can be dramatically improved by chemical reaction. A raw extrapolation of our results would predict that a polymer barrier membrane which prevents leakage for six months could ideally be made effective for half a century or more with the inclusion of reactive material. This improved effectiveness, however, is not guaranteed. First, it is necessary to identify a particular chemistry which can consume the contaminant sufficiently rapidly. Second, the ratio of the reaction rate to the diffusion rate must be large, i.e. the second Damköhler number must be much greater than one. Third, any reactive material must be accessible and must be completely consumed for the lag time to increase by the largest possible extent.

These assumptions are tested using eq 3 to predict the diffusion lag time for the Fe^0/PVA membranes. The required parameters (L, C_0, C_{up}, ν, P) are all known from the experiments, where P is obtained from a diffusion experiment using a pure PVA membrane for the reasons described above. Table 1 compares predicted lag times with experimental lag times. In all cases, predicted lag times are larger. The ratio of the predicted to experimental values is smallest for Cu^{2+} ($\cong$ 2), larger for carbon tetrachloride, nitrobenzene, and 4-nitroacetophenone ($\cong$ 6), and largest for CrO_4^{2-} ($\cong$ 13). This means that Cu^{2+} obeys eq 4 much better than CrO_4^{2-}.

This discrepancy is probably due to the fact that not all of the iron in the membrane was consumed by reaction with contaminants by the time of breakthrough. To determine how much of the iron is actually available for the reaction, C_0 in eq 3 is replaced by an "effective iron concentration", C_0^{eff} :

$$t_{lag} = \frac{L^2 C_0^{eff}}{2\nu P C_{up}} = \frac{L^2 C_0}{2\nu P C_{up}} \frac{C_0^{eff}}{C_0} \quad (4)$$

A plot of t_{lag} against $\frac{L^2 C_0}{2\nu P C_{up}}$ for each contaminant should give a straight line with the slope of $\frac{C_0^{eff}}{C_0}$, a fraction of iron accessible for the particular compound. Figure 7 shows such a plot applied to Cu^{2+} and carbon tetrachloride. The slope of the line is 0.45 for Cu^{2+} and 0.19 for carbon tetrachloride: only 45 % of the iron (based on the iron content in the dry membrane prior to hydration) was consumed by reaction with Cu^{2+} and 19 % by reaction with carbon tetrachloride. The same analysis shows that 25 %, 17 %, and 6 % of the iron was consumed by nitrobenzene, 4-nitroacetophenone, and CrO_4^{2-}, respectively. When accounting for the 40-47% of the iron lost during hydration of the membrane prior to conducting the breakthrough experiments, these percentages increase by approximately a factor of two. Considering these numbers, most of the iron in the membrane (about 90 %) was "consumed" before the breakthrough of Cu^{2+} occurs. For the other compounds, 50-70 % of the iron was "consumed" during the hydration and reaction periods. A large portion of the iron (> 30 %), however, is still unaccounted. Other possibilities for the difference between predicted and observed lag times include: oxidation of Fe^0 by reaction with water during the breakthrough experiment and formation of a surface reaction product film which reduces the reaction rate.

The presence of carbon tetrachloride during the diffusion experiment did not significantly increase the measured concentrations of dissolved iron. This implies that the iron oxidized by contaminants is not released into the solution but remains in the membrane as a solid oxide phase. This idea is supported by an SEM image of the

Fe^0/PVA membrane after the experiment in which the nanoparticles can be still seen (Supporting Information). Visual inspection of the membrane after exposure to carbon tetrachloride suggests that at least a portion of the iron remains in the membrane as an iron oxide, for the exposed area of the membrane is an orange/brown color common to iron oxide solids (Supporting Information). It is unlikely, however, that all of the "remaining iron" in the membrane is oxidized. The formation of an oxide layer will slow the reaction of oxidized contaminants with Fe^0 (41, 42), likely to a point where diffusion through the membrane becomes faster than reaction (i.e. the Damköhler number becomes small), and contaminant breakthrough occurs. Thus, we suspect that a large portion of the Fe^0 is covered by iron oxide and unavailable to the contaminants (carbon tetrachloride, nitrobenzene, and 4-nitroacetophenone) diffusing through the membrane. In the case of CrO_4^{2-}, the Fe^0 surface is likely covered by precipitated Cr_2O_3 as mentioned above, resulting in a similar effect.

One potential strategy to make a larger fraction of the iron accessible would be to use smaller iron particles. This method, however, has two disadvantages. The larger specific surface area could lead to faster reaction not only with contaminants but also with water. The difficulty and potential cost (43) associated with synthesis of smaller iron particles may be prohibitive as well.

Engineering Implications

Finally, the practical value of the results are discussed. The use of the Fe^0/PVA membranes even as a model barrier has two disadvantages. The iron reacts with water, and it is susceptible to oxidation in air. These problems are due to the large free volume in the PVA matrix. The hydrated PVA membrane is 50 % water by volume, which makes

PVA highly permeable to dissolved species. In engineering applications using less permeable materials such as HDPE, which would contain less than 0.03 wt% water (44), such problems will be much less important. As a result, the Fe^0 will be mainly used for reaction with contaminants, and the barrier membrane life will be much longer.

Thin Fe^0/PVA membranes are easy to synthesize and allow quick measurement of contaminant breakthrough. The method developed in this study, however, is universal. Results of this study can be extrapolated to Fe^0/HDPE membranes by using appropriate values of P and L. Such a calculation will likely give a conservative estimate of the lag time, because less oxidation of Fe^0 by water in the hydrophobic HDPE membrane would potentially lead to a larger $\frac{C_0^{eff}}{C_0}$, if the iron is not rendered inaccessible via a coating of insoluble iron corrosion products. Thin Fe^0/HDPE membranes are currently being developed to test this extrapolation.

Acknowledgements

This research was principally supported by the Environmental Management Science Program of the Office of Science, U.S. Department of Energy, grant DE-FG07-02ER63509. Other support came from the Institute of Hazardous Materials Management, the US Air Force (F49620-01-10333), the Petroleum Research Fund (39083-AC9), and the National Science Foundation (CTS 0322882). Appreciation is also extended to the reviewers for their careful attention, especially to the permeability results. Their efforts have greatly improved this contribution.

Supporting Information Available

SEM image of free Fe^0 nanoparticles, procedures to adjust a breakthrough curve for a PVA membrane with respect to C_{up} and L, EDS spectra of Fe^0/PVA membranes exposed

to Cu^{2+} and CrO_4^{2-}, SEM image of Fe^0/PVA membrane after reaction with carbon tetrachloride, and pictures of hydrated Fe^0/PVA membranes before/after a breakthrough experiment. This material is available free of charge via the Internet at http://pubs.acs.org.

Literature Cited

(1) Koerner, R. M. *Designing with Geosynthetics*; Prentice Hall: Upper Saddle River, NJ, 1998.

(2) LaGrega, M. D.; Buckingham, P. L.; Evans, J. C.; Environmental Resources Management *Hazardous Waste Management*; McGraw-Hill: New York, 2001.

(3) National Research Council *Alternatives for Ground Water Cleanup*; National Academy Press: Washington, D. C., 1994.

(4) Schwarzbauer, J.; Heim, S.; Brinker, S.; Littke, R. *Water Res.* **2002**, *36*, 2275-2287.

(5) Environmental Protection Agency *Final National Priorities List (NPL) Sites,* [Online] Available: http://www.epa.gov/superfund/sites/query/queryhtm/nplfin1.htm [May, 2003].

(6) Workman, J. P.; Keeble, R. L. In *Sanitary Landfilling: Process, Technology and Environmental Impact*; T.H. Christensen, R. Cossu, R. Stegmann, Eds.; Academic Press Inc.: San Diego, CA, 1989; pp 301-309.

(7) Rowe, R. K.; Fraser, M. J. In *Geoenvironmental 2000,* Vol. 1, New Orleans, LA, 1995; pp 270-284.

(8) Hsuan, G. Y. *Geotextiles Geomembranes* **2000**, *18*(1), 1-22.

(9) Rowe, R. K.; Hrapovic, L.; Kosaric, N. *Geosynthetics Int.* **1995**, *2*(3), 507-536.

(10) Rowe, R. K.; Hrapovic, L.; Armstrong, M. D. In *EUROGEO 1*, Maastricht, Netherlands, 1996; pp 737-742.

(11) Yang, C.; Nuxoll, E. E.; Cussler, E. L. *AIChE J.* **2001**, *47*(2), 295-302.

(12) Gillham, R. W.; O'Hannesin, S. F. *Ground Water* **1994**, *32*(6), 958-967.

(13) Matheson, L. J.; Tratnyek, P. G. *Environ. Sci. Technol.* **1994**, *28*, 2045-2053.

(14) Johnson, T. L.; Scherer, M. M.; Tratnyek, P. G. *Environ. Sci. Technol.* **1996**, *30*(8), 2634-2640.

(15) Orth, S. W.; Gillham, R. W. *Environ. Sci. Technol.* **1996**, *30*(1), 66-71.

(16) Roberts, L. A.; Totten, L. A.; Arnold, W. A.; Burris, D. R.; Campbell, T. J. *Environ. Sci. Technol.* **1996**, *30*(8), 2654-2659.

(17) Wang, C.; Zhang, W. *Environ. Sci. Technol.* **1997**, *31*(7), 2154-2156.

(18) Lien, H.; Zhang, W. *J. Environ. Eng.* **1999**, *125*(11), 1042-1047.

(19) Arnold, W. A.; Roberts, L., A. *Environ. Sci. Technol.* **2000**, *34*(9), 1794-1805.

(20) Agrawal, A.; Tratnyek, P. G. *Environ. Sci. Technol.* **1996**, *30*(1), 153-160.

(21) Devlin, J. F.; Klausen, J.; Schwarzenbach, R. P. *Environ. Sci. Technol.* **1998**, *32*(13), 1941-1947.

(22) Gould, J. P. *Water Res.* **1982**, *16*, 871-877.

(23) Khudenko, B. M.; Gould, J. P. *Water Sci. Technol.* **1991**, *24*(7), 235-246.

(24) Ku, Y.; Chen, C. *Separ. Sci. Technol.* **1992**, *27*(10), 1259-1275.

(25) Cantrell, K. J.; Kaplan, D. I.; Wietsma, T. W. *J. Hazard. Mater.* **1995**, *42*(2), 201-212.

(26) Pratt, A. R.; Blowes, D. W.; Ptacek, C. J. *Environ. Sci. Technol.* **1997**, *31*(9), 2492-2498.

(27) Puls, R. W. In *25th Annual Conference on Water Resources Planning and Management*; American Society of Civil Engineers: Chicago, IL, 1998; pp 116-121.

(28) Alowitz, M. J.; Scherer, M. M. *Environ. Sci. Technol.* **2002**, *36*(3), 299-306.

(29) Crank, J. *The Mathematics of Diffusion*; Clarendon Press: Oxford, UK, 1975.

(30) Schrick, B.; Blough, J. L.; Jones, D. A.; Mallouk, T. E. *Chem. Mater.* **2002**, *14*(12), 5140-5147.

(31) Stookey, L. L. *Anal. Chem.* **1970**, *42*(7), 779-781.

(32) Gibbs, C. R. *Anal. Chem.* **1976**, *48*(8), 1197-1201.

(33) O'Sullivan, D. W. *UV/Vis Determination of Iron in Cereal*, [Online] Available: http://www.chemistry.usna.edu/dano/web_info/sc306/UVVis_Iron.pdf [May, 2003].

(34) Scancar, J.; Milacic, R.; Strazar, M.; Burica, O. *Sci. Total Environ.* **2000**, *250*(1-3), 9-19.

(35) Environmental Protection Agency *Design, Operation, and Closure of Municipal Solid Waste Landfills*; Cincinnati, OH, 1994; EPA/625/R-94/008.

(36) American Public Health Association; American Water Works Association; Water Pollution Control Federation *Standard Methods for the Examination of Water and Wastewater: Including Bottom Sediments and Sludges*; American Public Health Association: New York, 1998.

(37) Siegel, R. A.; Cussler, E. L. *J. Membr. Sci.* accepted for publication.

(38) Melitas, N.; Chuffe-Moscoso, O.; Farrell, J. *Environ. Sci. Technol.* **2001**, *35*(19), 3948-3953.

(39) Duncalf, B.; Dunn, A. S. *J. Appl. Polym. Sci.* **1964**, *8*, 1763-1776.

(40) Van Nice, L. H.; Farlee, R. *Polym. Sci. Eng.* **1977**, *17*(6), 359-365.

(41) Scherer, M. M.; Westall, J. C.; Ziomek-Moroz, M.; Tratnyek, P. G. *Environ. Sci. Technol.* **1997**, *31*(8), 2385-2391.

(42) Farrell, J.; Kason, M.; Melitas, N.; Li, T. *Environ. Sci. Technol.* **2000**, *34*(3), 514-521.

(43) Easom, K. A.; Klabunde, K. J.; Sorensen, C. M. *Polyhedron* **1994**, *13*(8), 1197-1223.

(44) Eloy-Giorni, C.; Pelte, T.; Pierson, P.; Margrita, R. *Geosynthetics Intl.* **1996**, *3*(6), 741-769.

Table 1. Summary of the breakthrough experiments

contaminant	Iron C_0 (M)[a]	upstream solute conc., C_{up} (μM)	downstream volume, V_{down} (mL)	membrane thickness, L (μm)	P ($\times 10^{-9}$ m^2/min)	observed t_{lag} (min)	predicted t_{lag}[c] (min)	$\frac{\text{predicted } t_{lag}}{\text{observed } t_{lag}}$ (-)
Cu^{2+}	0	5004	13.11	133	2.68[d]	1.74[b]	-	-
Cu^{2+}	0.44	5343	13.11	157	2.15	178.2	374	2.10
Cu^{2+}	0.44	1018	13.11	200	2.68	1352.4	3186	2.36
Cu^{2+}	0.44	2002	13.11	195	1.28	837.6	1540	1.84
Cu^{2+}	1.25	2995	13.11	102	2.45	373.8	809	2.17
carbon tetrachloride	0	146	16.64	198	2.65[d]	1.04[b]	-	-
carbon tetrachloride	1.24	4562	16.64	212	2.13	353	1818	5.15
carbon tetrachloride	1.24	3864	16.64	140	7.67	165	936	5.67
CrO_4^{2-}	0	1598	13.11	295	1.79[d]	45.4[b]	-	-
CrO_4^{2-}	0.44	5014	13.11	164	4.08	35.2	435	12.36
CrO_4^{2-}	1.25	2512	13.11	113	2.26	86.9	1185	13.64
nitrobenzene	0	1669	13.11	88	4.31[d]	0.54[b]	-	-
nitrobenzene	1.25	4692	13.11	127	8.07	28.2	166	5.89
nitrobenzene	1.27	2020	13.11	80	5.30	52.6	155	2.95
4-nitroacetophenone	0	1102	13.11	79	3.07[d]	0.51[b]	-	-
4-nitroacetophenone	0.41	2424	13.11	82	5.37	9.5	61.7	6.50
4-nitroacetophenone	1.27	1997	13.11	89	6.27	45.9	272	5.92

[a]Iron concentration in the membrane is based on wet volume.

[b]These values are not adjusted with respect to L or C_{up} (see Supporting Information). Adjusted values are given in the text.

[c]The lag time was estimated using eq 3.

[d]These permeability values for the pure PVA membranes were used to calculate the predicted t_{lag} for the Fe^0/PVA membranes using eq 3.

Figure Captions

Figure 1. Conceptual breakthrough curves for reactive and non-reactive membranes. C_{down} = downstream concentration of a contaminant, t = time, t_{lag} = breakthrough lag time, L = membrane thickness, D = diffusion coefficient of the contaminant in the membrane, C_0 = concentration of a reactive material in the membrane at the beginning of a diffusion experiment, C_{up} = upstream concentration of a contaminant, ν = stoichiometric coefficient of the reaction, and P = permeability of the membrane for the specific contaminant.

Figure 2. SEM images of (a) a dry PVA membrane surface and (b) a dry Fe^0/PVA membrane surface before the breakthrough experiment. Black spots are nanoparticles of Fe^0. Surface roughness is also observed as ridges. Images were inverted and adjusted for brightness and contrast using Adobe Photoshop v.5.0.2.

Figure 3. The experimental setup for the diaphragm-cell diffusion experiments: (a) closed-cell and (b) flow-cell experiments.

Figure 4. Typical breakthrough curves for carbon tetrachloride with pure PVA membranes. The downstream concentration (C_{down}) is normalized by the initial upstream concentration (C_{up}). V_{down} and A are the downstream cell volume and the membrane cross-sectional area available for diffusion, respectively. The two experiments (●, L = 198 μm, C_{up} = 146 μM, V_{down} = 16.64 mL; ○, L = 44 μm, C_{up} = 131 μM, V_{down} = 13.11

mL) used membranes with different thicknesses. The regressed, dashed lines are related to the steady-state flux.

Figure 5. Variation of permeance with reciprocal membrane thickness. Error bars associated with the data points (●) indicate the standard deviation based on replicates using the same membrane. The data points without error bars (▼) were not replicated. The dashed line represents a linear regression with zero intercept ($R^2 = 0.93$).

Figure 6. The breakthrough curves through PVA (●) and Fe^0/PVA (○) membranes: (a) carbon tetrachloride (C_{up} = 4562 μM, L = 212 μm, V_{down} = 16.64 mL), (b) Cu^{2+} (C_{up} = 2995 μM, L = 102 μm, V_{down} = 13.11 mL), (c) nitrobenzene (C_{up} = 2020 μM, L = 80 μm, V_{down} = 13.11 mL), (d) 4-nitroacetophenone (C_{up} = 2424 μM, L = 89 μm, V_{down} = 13.11 mL), and (e) CrO_4^{2-} (C_{up} = 2512 μM, L = 113 μm, V_{down} = 13.11 mL). The dashed lines are related to the steady-state flux. Note the different concentration and time scales.

Figure 7. Dependence of the breakthrough lag time on the aggregated parameter $C_0L^2/(2\nu PC_{up})$ for carbon tetrachloride (Δ) and Cu^{2+} (●). The dashed lines are linear regressions with their y-intercept fixed at the lag time for the pure PVA membrane (R^2 = 0.996 for Δ and 0.977 for ●).

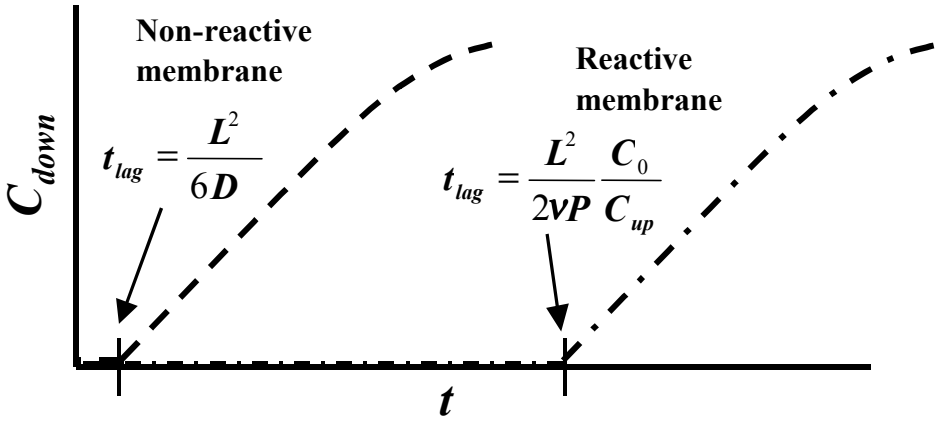
Non-reactive membrane
$t_{lag} = \frac{L^2}{6D}$
Reactive membrane
$t_{lag} = \frac{L^2}{2\nu P}\frac{C_0}{C_{up}}$
C_{down}
t

Figure 1

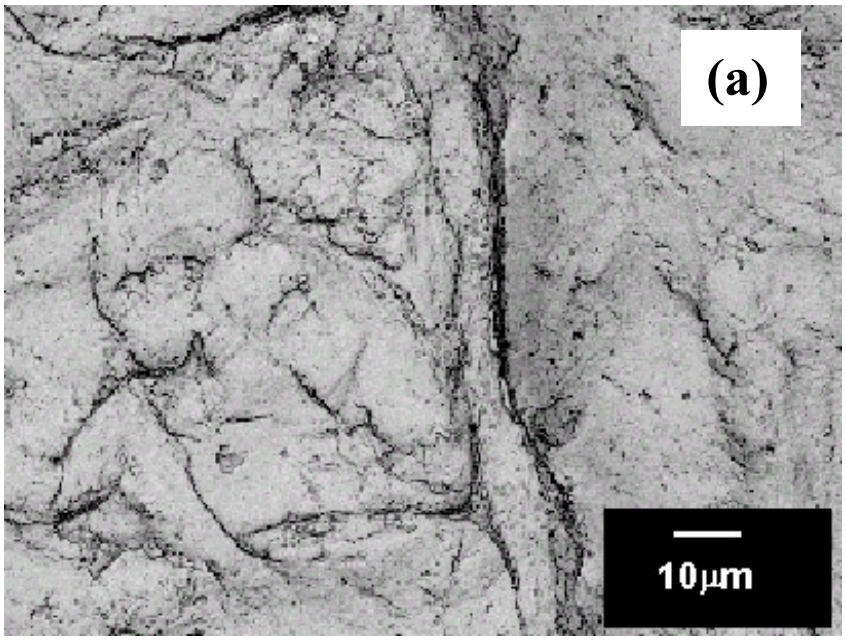

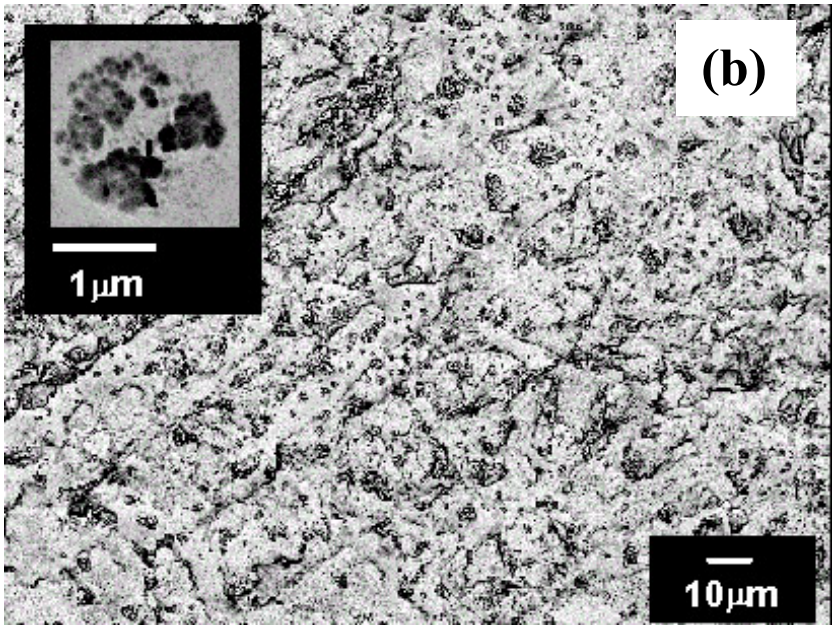

Figure 2

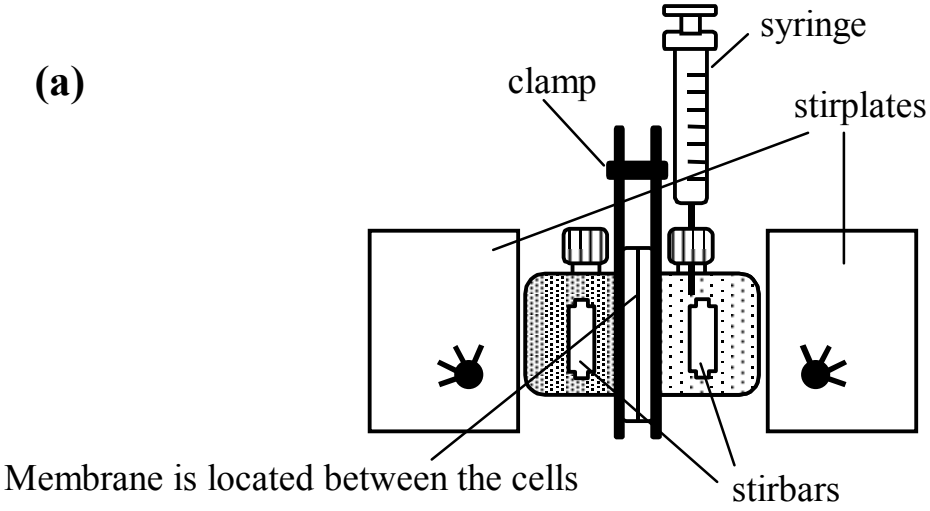
(a)
syringe
clamp
stirplates
Membrane is located between the cells
stirbars

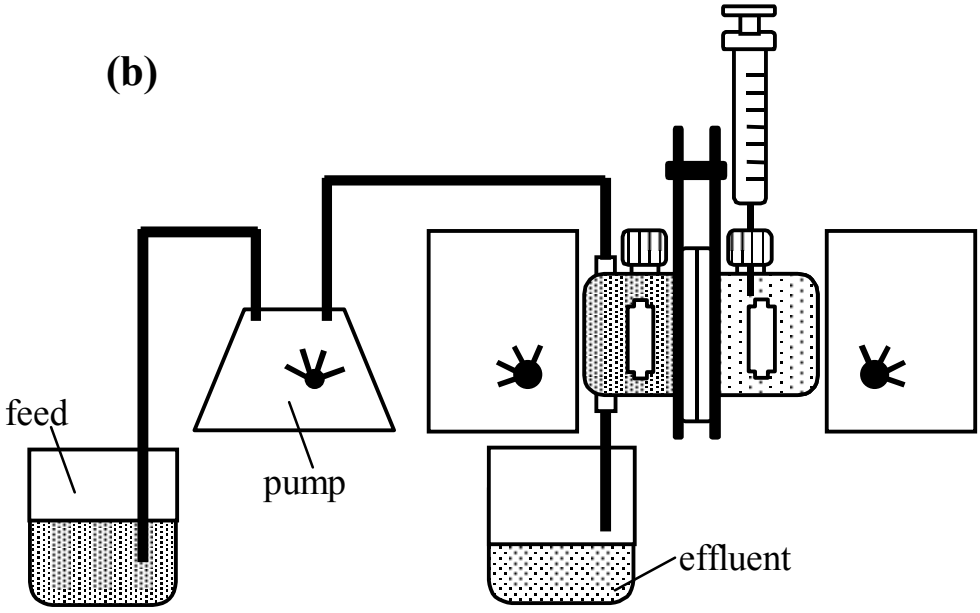
(b)
feed
pump
effluent

Figure 3

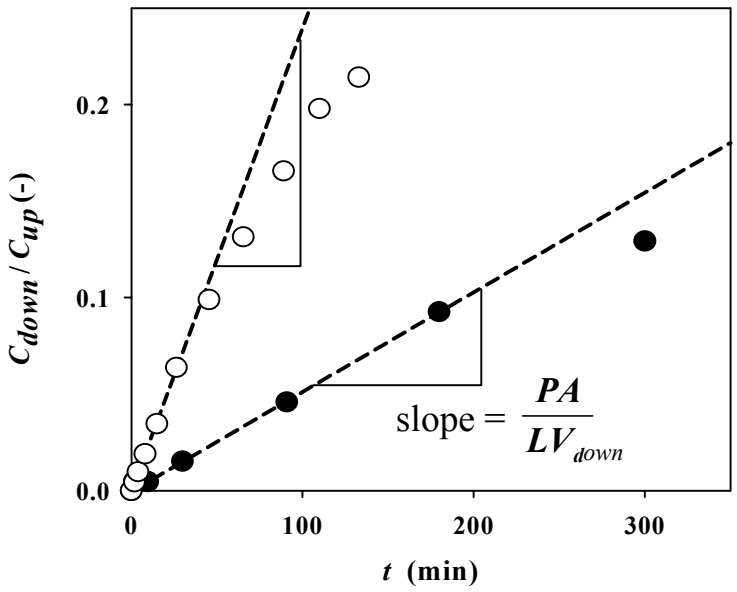

Figure 4

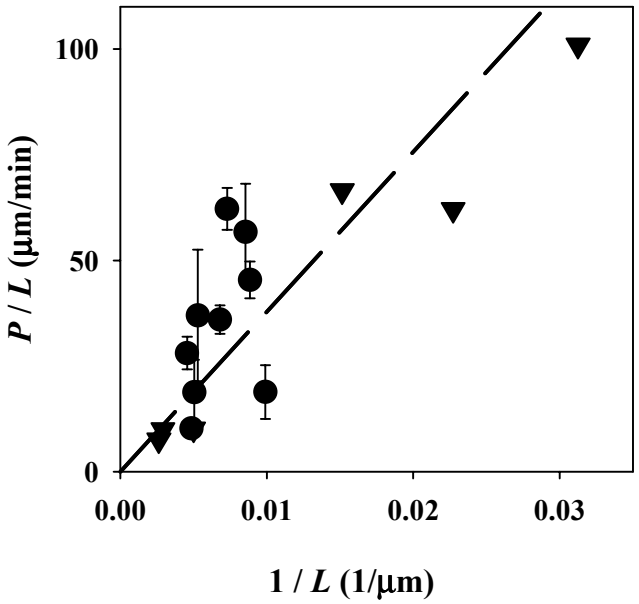

Figure 5

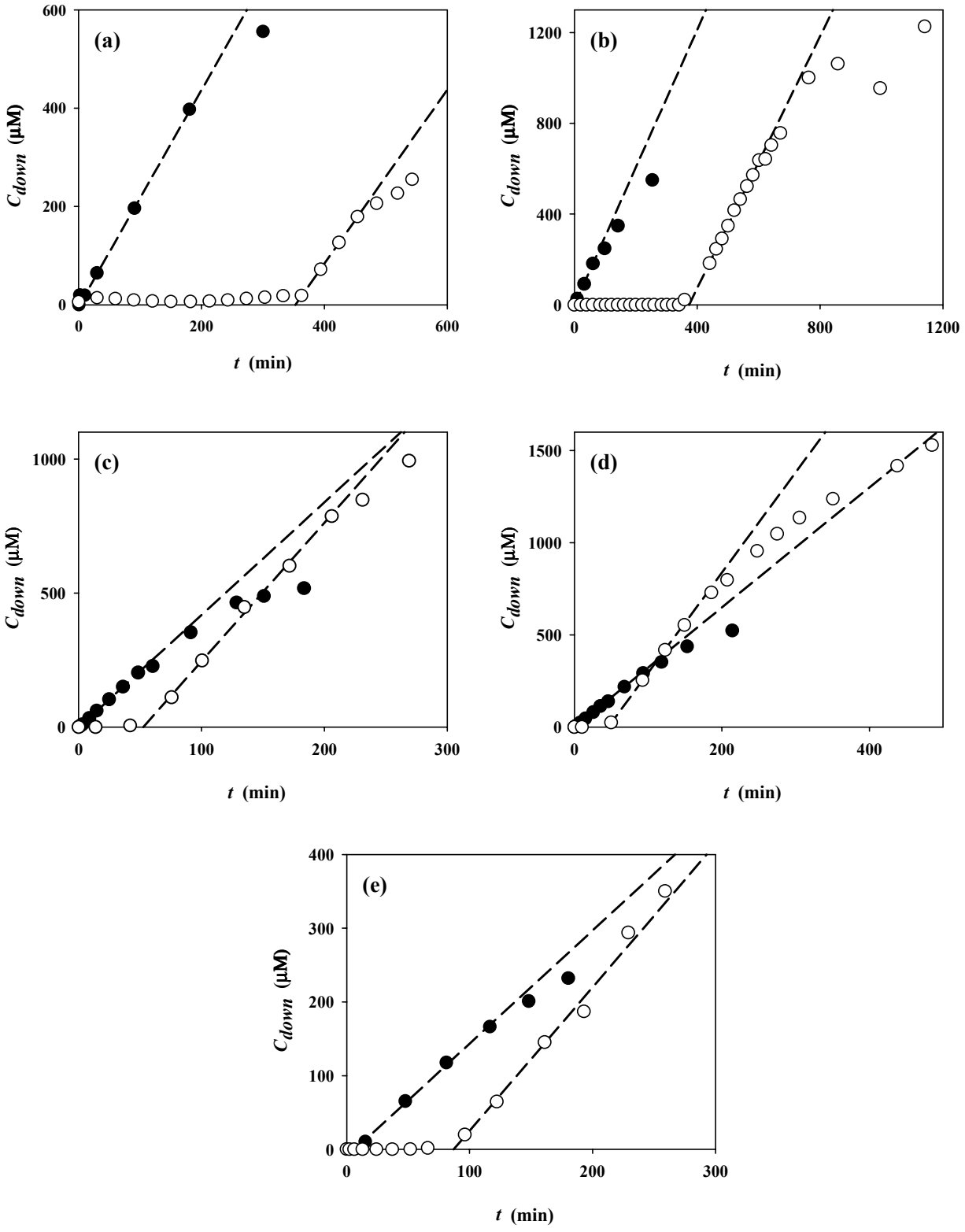
(a)
(b)
(c)
(d)
(e)
C_{down} (μM)
t (min)
0
200
400
600
800
1000
1200
1500
100
300
500

Figure 6

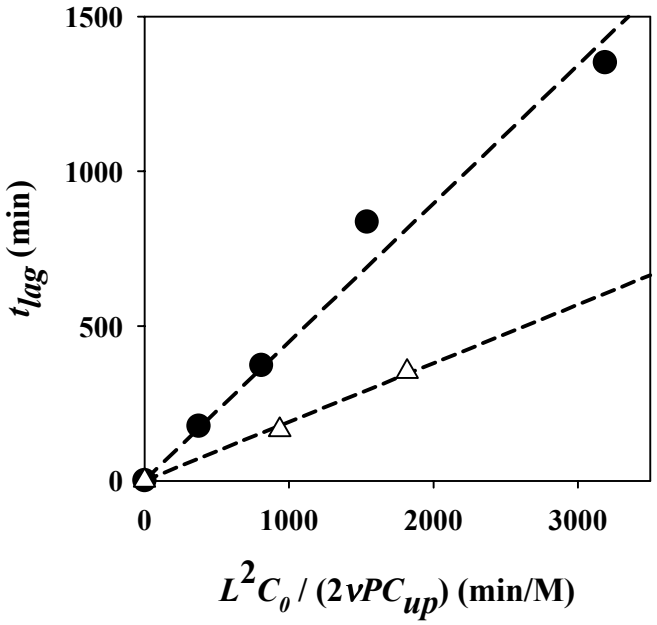

Figure 7